LAWRENCE
LIVERMORE
NATIONAL
LABORATORY

LLNL-JRNL-414165

X-RAY PHOTOEMISSION ANALYSIS OF CHEMICALLY TREATED GaTe SEMICONDUCTOR SURFACES FOR RADIATION DETECTOR APPLICATIONS

Art J. Nelson, Adam M. Conway, B.W. Sturm, E.M. Behymer, C.E Reinhardt, R.J. Nikolic, S.A. Payne, G. Pabst , K. C. Mandal

June 24, 2009

Journal of Applied Physics

Disclaimer

X-RAY PHOTOEMISSION ANALYSIS OF CHEMICALLY TREATED GaTe SEMICONDUCTOR SURFACES FOR RADIATION DETECTOR APPLICATIONS

A.J. Nelson, A.M. Conway, B.W. Sturm, E.M. Behymer, C.E Reinhardt, R.J. Nikolic, and S.A. Payne
Lawrence Livermore National Laboratory, Livermore, CA, USA.

G. Pabst and K. C. Mandal
EIC Laboratories, Inc., 111 Downey Street, Norwood, MA 02062

Abstract

The surface of the layered III-VI chalcogenide semiconductor GaTe was subjected to various chemical treatments commonly used in device fabrication to determine the effect of the resulting microscopic surface composition on transport properties. Various mixtures of H_3PO_4:H_2O_2:H_2O were accessed and the treated surfaces were allowed to oxidize in air at ambient temperature. High-resolution core-level photoemission measurements were used to evaluate the subsequent chemistry of the chemically treated surfaces. Metal electrodes were created on laminar (cleaved) and nonlaminar (cut and polished) GaTe surfaces followed by chemical surface treatment and the current versus voltage characteristics were measured. The measurements were correlated to understand the effect of surface chemistry on the electronic structure at these surfaces with the goal of minimizing the surface leakage currents for radiation detector devices.

INTRODUCTION

The layered III-VI chalcogenide semiconductor GaTe has potential for room temperature gamma ray spectroscopy applications due to its 1.57 eV band gap and high atomic numbers. [1,2] Attempts to fabricate working room temperature radiation detectors using high-resistivity GaTe substrates have precipitated the need to engineer the chemical states at the metal/semiconductor interface. Controlling the oxidation state at this interface will impact the device transport properties and thus an appropriate surface preparation needs to be developed.

Mechanical polishing followed by chemical etching is routinely employed for surface preparation prior to device fabrication. However, alternative surface preparation methods need to address surface passivation of defect states. Surface passivation of III-V compound semiconductor surfaces is well documented [3] as a means to address the detrimental effects coming from high-density surface states and related Fermi level pinning. Similar surface treatments related to II-VI binary and I-III-VI ternary semiconductor devices have been explored only recently. [4-10]

In this work, various wet chemical treatments with H_3PO_4:H_2O_2:H_2O, H_3PO_4:H_2O, H_2O_2:H_2O were accessed. The chemical processing of the GaTe surface is examined in detail by interrupting the treatment cycle and characterizing with monochromatic x-ray photoelectron spectroscopy (XPS) to examine the surface reactions associated with each separate chemical treatment. The treated surfaces were allowed to oxidize in air at ambient temperature for timed intervals and characterizing the surface after each timed exposure in order to monitor the growth of any oxide layer. Current-voltage (I-V) measurements were acquired after metalizing, chemically treating the

exposed surface and correlating the results with the surface chemistry.

EXPERIMENTAL

GaTe crystals were grown at EIC Laboratories using stoichiometric amounts of high purity (7N) Ga and zone refined Te as starting materials to make a homogeneous polycrystalline ingot. The polycrystalline ingot was encapsulated in Struers Epofix for metallographic sample preparation. Sequential polishing of the GaTe with finer and finer diamond paste followed by colloidal silica resulted in a surface with a mirror finish and rms surface roughness of 20 nm as determined with Zygo optical interferometry. Wet etching of the polished GaTe laminar surface was performed using various mixtures of H_3PO_4, H_2O_2 and H_2O. Specifically, H_3PO_4:H_2O_2:H_2O with the ratio of 1:1:10 by volume respectively, H_3PO_4:H_2O (1:10) and H_2O_2:H_2O (1:10). Following each treatment cycle, the samples were rinsed in DI water and blown dry with N_2. XPS was used to investigate the surface chemistry after each treatment cycle in an effort to understand the effect of surface composition on room temperature radiation detector performance.

XPS analysis was performed on a PHI Quantum 2000 system using a focused monochromatic Al Kα x-ray (1486.7 eV) source for excitation and a spherical section analyzer. The instrument has a 16-element multichannel detection system. A 100 μm diameter x-ray beam was used for analysis. The x-ray beam is incident normal to the sample and the x-ray detector is at 45° away from the normal. The pass energy was 23.5 eV giving an energy resolution of 0.3 eV that when combined with the 0.85 eV full width at half maximum (FWHM) Al Kα line width gives a resolvable XPS peak width of 1.2 eV FWHM. Deconvolution of non-resolved peaks was accomplished using Multipak

6.1A (PHI) curve fitting routines. The collected data were referenced to an energy scale with binding energies for Cu $2p_{3/2}$ at 932.72± 0.05 eV and Au $4f_{7/2}$ at 84.01± 0.05 eV. Binding energies were also referenced to the C 1s photoelectron line arising from adventitious carbon at 284.8 eV. Low energy electrons and argon ions were used for specimen neutralization.

The effect of the aforementioned chemical treatments on surface conductivity was studied on both the nonlaminar and laminar surface of GaTe sample. The nonlaminar surface was prepared using the cutting and polishing procedure described above, and the laminar surface was prepared by cleaving. Gold electrode patterns were fabricated using standard photolithography and lift off processes. TLM patterns were used to evaluate the change in sheet resistance of the material and circular diode patterns were used to measure the change in bulk current after each treatment which is shown schematically in Figure 1. Current vs. voltage measurements were performed on the TLM patterns and diodes as fabricated, after 1 minute in H_3PO_4:H_2O (1:10), after 1 minutes in H_2O_2 (30% dilute), and finally a H_3PO_4:H_2O_2:H2O (1:1:10) treatment for 5 minutes.

A wet etching experiment of GaTe was performed using a mixture of H_3PO_4, H_2O_2 and H_2O with the ratio of 1:1:10 by volume respectively. To create a pattern on the sample to use as an etch mask, photolithography, followed e-beam evaporation of 200 nm of Au and finally liftoff of the unwanted metal portions was performed on a laminar face of the GaTe sample. The experiment consisted of exposing the sample to the etchant for durations of 1, 2, and 5 minutes and measuring the step height with a surface profilometer in between each etch step to determine the etch rate and surface roughness. This etchant functions by oxidizing the GaTe via the H_2O_2 followed by etching with H_3PO_4. The etch

rate of the GaTe non-laminar surface for: various concentrations of the solution (abscissa), the effect of stirring, and crystallographic direction was determined. In all experiments, the reaction was conducted in room light and the solution was at room temperature.

RESULTS AND DISCUSSION

XPS survey spectra of the as treated GaTe laminar surfaces were acquired to determine surface stoichiometry and impurity concentrations. The quantitative surface compositional analyses and elemental ratios are summarized in Tables I-III. The Ga/Te ratio indicates that the as received laminar surface is Te-rich. Compositional analysis following the 5 min. H_3PO_4:H_2O_2:H_2O treatment reveals less oxygen and a Ga/Te ratio indicative of a Te-rich surface. The 1 min. H_3PO_4:H_2O treatment also results in a Te-rich surface while the H_2O_2:H_2O treatment initially results in a more stoichiometric oxidized surface. These as treated surfaces were exposed to air and allowed to react then further characterized as described below.

Photoemission measurements on the Ga 2p, Te 3d and O 1s core lines were used to further evaluate the chemical bonding on the as treated surfaces at each cycle of the process and after subsequent oxidation. Beginning with the as received polished surface, the Ga $2p_{3/2}$ peak binding energy is 1118.4 eV, which is representative of Ga_2O_3. The Te 3d spectrum shown in Figure 1 for the as received GaTe surface shows two sets of Te $3d_{5/2,3/2}$ spin-orbit pairs. The higher binding energy Te $3d_{5/2}$ peak at 576.3 eV represents Te^{4+} in TeO_2 (E_g = 3.5 eV) and the lower binding energy peak at 573 eV represents lattice bound Te in GaTe. [10, 11] In addition, the O 1s peak has two components with 530.8

and 532.8 eV binding energies attributed to Ga_2O_3 and TeO_2, respectively. The binding energies for the photoelectron peaks are summarized in Table IV.

After 1 minute in the H_3PO_4:H_2O_2:H_2O solution, the GaTe surface becomes fully oxidized as evidenced by the Te $3d_{5/2}$ peak at 576.4 eV indicative of Te^{4+} in TeO_2 and the absence of the lower binding energy component. The lower binding energy Te $3d_{5/2}$ peak reappears following 3 minutes in the H_3PO_4:H_2O_2:H_2O solution. Finally, after 5 minutes in the H_3PO_4:H_2O_2:H_2O solution, the GaTe surface is oxide free as evidenced by the sole Te $3d_{5/2}$ peak at 572.9 eV. Based on this data we conclude that the H_3PO_4:H_2O_2:H_2O solution first oxidizes the GaTe surface and then completely removes the oxide leaving a pristine surface ideal for metal contact application.

The stability of the H_3PO_4:H_2O_2:H_2O treated GaTe surface was quantitatively measured by allowing the etched GaTe surface to oxidize in air at ambient temperature for timed intervals and characterizing the surface after each timed exposure. Monitoring the growth of the oxide was thus accomplished using the components of the Te $3d_{5/2}$ peak and their respective binding energies.

From Figure 2 we note that minimal oxide growth has occurred on the etched GaTe surface after 5 minutes in ambient air. However, after 10 min. in air, a small Te $3d_{5/2}$ component indicative of TeO_2 begins to appear at 576.9 eV. This oxide peak continues to grow after each air exposure but never attains its original 'as received' intensity. This data suggests that the H_3PO_4:H_2O_2:H_2O solution treatment initially passivates the GaTe surface.

To further elucidate the oxidation/reduction mechanism of the H_3PO_4:H_2O_2:H_2O solution on the GaTe surface, H_3PO_4:H_2O and H_2O_2:H_2O solutions were used separately.

Figure 3 shows the progression of Te surface chemical bonding at each timed treatment cycle. After 1 minute in the H_3PO_4:H_2O solution, the GaTe surface is oxide free as evidenced by the sole Te $3d_{5/2}$ peak at 573.2 eV. Allowing the surface to oxidize in air at ambient temperature for timed intervals, we note that minimal oxide growth has occurred on the etched GaTe surface after 15 minutes in ambient air. However, after 35 min. in air, a Te $3d_{5/2}$ component indicative of TeO_2 begins to appear at 576.3 eV. This oxide peak continues to grow after further air exposure but again never attains its original 'as received' intensity. This data suggests that the H_3PO_4:H_2O solution alone can be used to effectively passivate the GaTe surface.

The progression of Te surface chemical bonding for the H_2O_2:H_2O solution is presented in Figure 4. After 1 minute in the H_2O_2:H_2O solution, the as received GaTe surface is further oxidized as evidenced by the increased intensities of the Te $3d_{5/2}$ peak indicative of surface oxide. Compositional analysis revealed that this is a more stoichiometric surface than the as received surface. A 3 min. or 5 min. treatment in H_2O_2:H_2O yields a fully oxidized surface initially forming a mixture of Ga_2O_3/TeO_2 or $GaTeO_3$ that may prove ideal for Schottky contacts on GaTe.

The measurements of the I-V characteristics for these H_3PO_4:H_2O_2:H_2O, H_3PO_4:H_2O, and H_2O_2:H_2O treated surfaces reveals that Au forms an ohmic contact, figure 5. A comparison of the sheet resistance and diode resistance after each chemical treatment for the laminar and nonlaminar surface is shown in figure 6. Similar trends are observed for both measurements, namely after phosphoric acid treatment the effective resistance decreases, possibly due to the removal of a passivating native oxide as was shown in above using XPS. Following the hydrogen peroxide treatment, a stable surface

TeO_x is formed which increases the effective resistance by acting as surface passivation. The surface and bulk components of the diode current for the laminar diodes were determined by measuring electrodes of various diameters, using the relationship:

$$J_{rtot}=J_a+J_p*P/A \qquad \text{(Eq. 1)}$$

where J_{rtot} is the total current density in A/cm^2, J_a is bulk component of the current density in A/cm^2, J_p is the periphery component in A/cm, P is the electrode periphery in cm and A is the electrode area in cm^2. The components are determined by plotting the total electrode current density at a fixed voltage as a function of P to A ratio for various size electrodes (Fig. 7), where the slope is equal to the periphery component and the intercept is the bulk component, show in Table V. The bulk component stays relatively constant (max 2x change) with surface treatment where as the periphery component varies by 10x.

The etch rates for various concentrations of etchant are shown in Figure 8. We find that the etch rate was 0-50 Å/sec depending on chemical concentration, and that the etch rate was not influenced by the crystallographic orientation in the nonlaminar direction. In addition, we did not observe a statistically relevant increase in etch rate with stirring, suggesting the kinetics are not diffusion-limited but rather reaction-limited. The etch rate along the laminar direction is 3x faster than the nonlaminar direction as evidenced by the SEM of the post etch electrode in Figure 9.

CONCLUSIONS

Wet chemical treatments can be used to affect GaTe surface chemistry and oxide

formation. Various mixtures of H_3PO_4:H_2O_2:H_2O were accessed and the treated surfaces were allowed to oxidize in air at ambient temperature. High-resolution photoemission measurements on the Ga 2p, Te 3d, and O 1s core lines were used to evaluate the subsequent chemistry of the chemically treated surfaces. The measured I-V characteristics were correlated with XPS results to understand the effect of surface chemistry on the electronic structure at these surfaces with the goal of minimizing the surface leakage currents for radiation detector devices. Fabrication of room temperature semiconductor radiation detectors should include thoughts on optimizing the metal contact to oxide/semiconductor structure for Schottky barrier engineering as well as to reduce surface leakage currents.

ACKNOWLEDGEMENTS

The authors would like to thank J. Go and E. Sedillo for metallographic sample preparation. This work was performed under the auspices of the U.S. Department of Energy by Lawrence Livermore National Laboratory under Contract DE-AC52-07NA27344.

References

1. M. Abdel Rahman and A.E. Belal, J. Phys. and Chem. of Solids **61** , 925 (2000).

2. A. M. Conway, C. E. Reinhardt, R. J. Nikolic, A. J. Nelson, T. F. Wang, K. J. Wu, S. A. Payne, K. C. Mandal, A. Burger, IEEE Nuclear Science Symposium (2008).

3. H. Hasegawa and M. Akazawa, Appl. Surf. Sci. **255**, 628 (2008).

4. A.J. Nelson, C. R. Schwerdtfeger, G.C. Herdt, D. King, M. Contreras and K. Ramanathan, J. Vac. Sci. Technol. **A15(4)**, 2058 (1997).

5. A.J. Nelson, L. Gregoratti, E. Chagarov, D. Lonza, M. Marsi and M. Kiskinova, Appl. Surf. Sci. **140/1-2**, 208 (1999).

6. K.-T. Chen, D. T. Shi, H. Chen, B. Granderson, M. A. George, W. E. Collins, and A. Burger, J. Vac. Sci. Technol. **A15(3)**, 850 (1997).

7. S. Wenbin, W. Kunshu, M. Jiahua, T. Jianyong, Z. Qi and Q. Yongbiao, Semicond. Sci. Technol. **20 ,** 343 (2005).

8. V. G. Ivanitska, P. Moravec, J. Franc, Z. F. Tomashik, P. I. Feychuk, V. M. Tomashik, L. P. Shcherbak, K. Masek, and P. Hoschl, J. Electron. Mater. **36(8)**, 1021 (2007).

9. L. Qiang and J. Wanqi, Nucl. Instrum. Methods A **562(1)**, 468 (2006).

10. A.J. Nelson, A.M. Conway, C.E. Reinhardt, J.L. Ferreira, R.J. Nikolic, and S.A. Payne, Materials Lett. **63**, 180 (2009).

11. O.A. Balitskii, W. Jaegermann, Materials Chemistry and Physics 97, 98–101 (2006).

Figure Captions

Figure 1. Schematic diagram of TLM patterns and diodes used in surface treatment experiments.

Figure 2. XPS Te 3d spectra for H_3PO_4:H_2O_2:H_2O etched and oxidized GaTe.

Figure 3. XPS Te 3d spectra for H_3PO_4:H_2O etched and oxidized GaTe.

Figure 4. XPS Te 3d spectra for H_2O_2:H_2O oxidized GaTe.

Figure 5. Current versus voltage characteristics of 100um diameter Au-GaTe-Au diodes before and after various treatments.

Figure 6. Normalized sheet and diode resistances after the various surface treatments for laminar and non-laminar surfaces. The resistances are normalized to the pre surface treatment resistance for each case.

Figure 7. Current density versus electrode periphery to area ratio for various chemical treatments.

Figure 8. Etch rate for the non-laminar surface and the effect of chemical concentration, crystallographic direction and use of stirring. Inset: Low magnification SEM image of the GaTe surface used for wet chemical etching experiments. A square photoresist pattern was used for surface profilometry to determine the etch rate.

Figure 9. SEM picture of H_3PO_4:H_2O_2:H_2O (1:1:10) etched GaTe.

Table I. Relative XPS Surface Compositional Analysis (atomic %) of the H_3PO_4:H_2O_2:H_2O treated and air exposed GaTe

Sample	Ga	Te	O	Ga/Te ratio
as received	9.8	28.6	61.6	0.34
1 min H_3PO_4:H_2O_2:H_2O	5.3	10.5	84.2	0.50
3 min H_3PO_4:H_2O_2:H_2O	11.3	32.5	56.2	0.35
5 min H_3PO_4:H_2O_2:H_2O	18.1	58.7	23.2	0.31
5 min air exposure	18.2	45.1	36.7	0.40
10 min air exposure	8.5	31.1	60.4	0.27
20 min air exposure	4.5	41.4	54.1	0.11
40 min air exposure	4.0	38.8	57.2	0.10
80 min air exposure	7.9	37.2	54.9	0.21

Table II. Relative XPS Surface Compositional Analysis (atomic %) of the H_3PO_4: H_2O treated GaTe

Sample	Ga	Te	O	Ga/Te ratio
as received	9.8	28.6	61.6	0.34
1 min H_3PO_4:H_2O	6.8	34.1	59.1	0.20
5 min in air	6.2	35.5	58.3	0.17
15 min in air	11.5	29.9	58.6	0.38
35 min in air	7.4	38.6	54.0	0.19
75 min in air	5.7	37.7	56.6	0.15

Table III. Relative XPS Surface Compositional Analysis (atomic %) of the H_2O_2:H_2O treated GaTe

Sample	Ga	Te	O	Ga/Te ratio
as received	9.8	28.6	61.6	0.34
1 min H_2O_2:H_2O	17.9	20.4	61.7	0.88
3 min H_2O_2:H_2O	29.8	13.9	56.3	2.14
5 min H_2O_2:H_2O	28.8	14.2	57.0	2.03

Table IV. Summary of XPS binding energies (eV) for the H_3PO_4:H_2O_2:H_2O processed and air exposed GaTe.

GaTe	Ga $2p_{3/2}$	Te $3d_{5/2}$	O 1s
As received	1118.4	573.0, 576.3	530.8, 532.8
1 min etch	1118.4	576.4	531.8, 533.1
3 min etch	1118.9	573.0, 576.6	531.4, 533.0
5 min etch	1119.4	572.9	–
5 min air exposure	1119.2	573.1	–
10 min air exposure	1119.4	573.2, 576.9	–
20 min air exposure	1119.3	573.1, 576.8	531.0, 532.3
40 min air exposure	1119.4	573.1, 576.5	531.0, 532.3
80 min air exposure	1119.1	573.0, 576.4	530.6, 532.1

Table V. Area and periphery components of current density for treated samples.

Surface Treatment	Ja	Jp
Pre Treatment	0.00159	5.20508E-5
H_3PO_4	0.07414	1.86319E-4
H_2O_2	0.00248	1.16429E-5

Figure 1

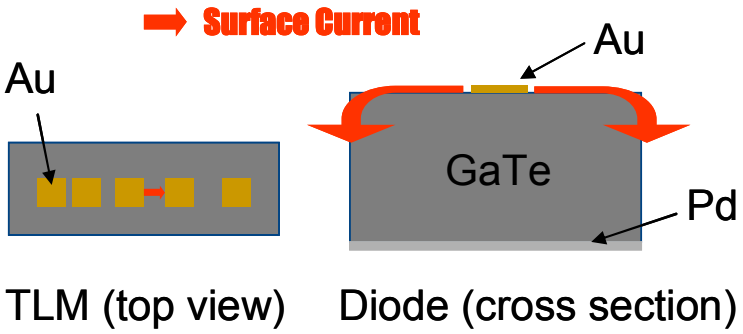
Surface Current
Au
Au
GaTe
Pd
TLM (top view)
Diode (cross section)

Figure 2

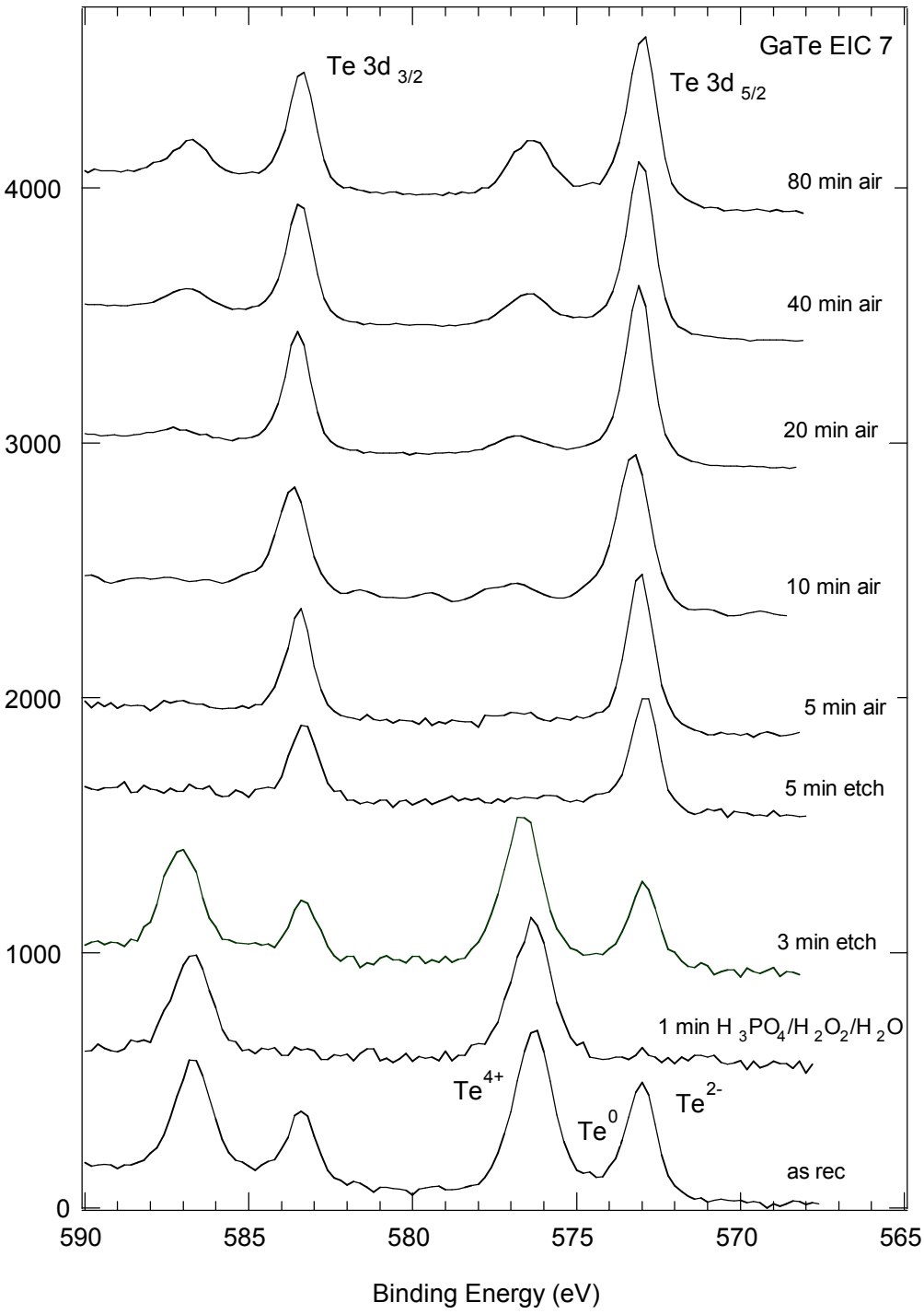
GaTe EIC 7
Te 3d 3/2
Te 3d 5/2
80 min air
40 min air
20 min air
10 min air
5 min air
5 min etch
3 min etch
1 min H 3PO4/H 2O2/H 2O
as rec
Te4+
Te0
Te2-
4000
3000
2000
1000
0
590
585
580
575
570
565
Binding Energy (eV)

Figure 3

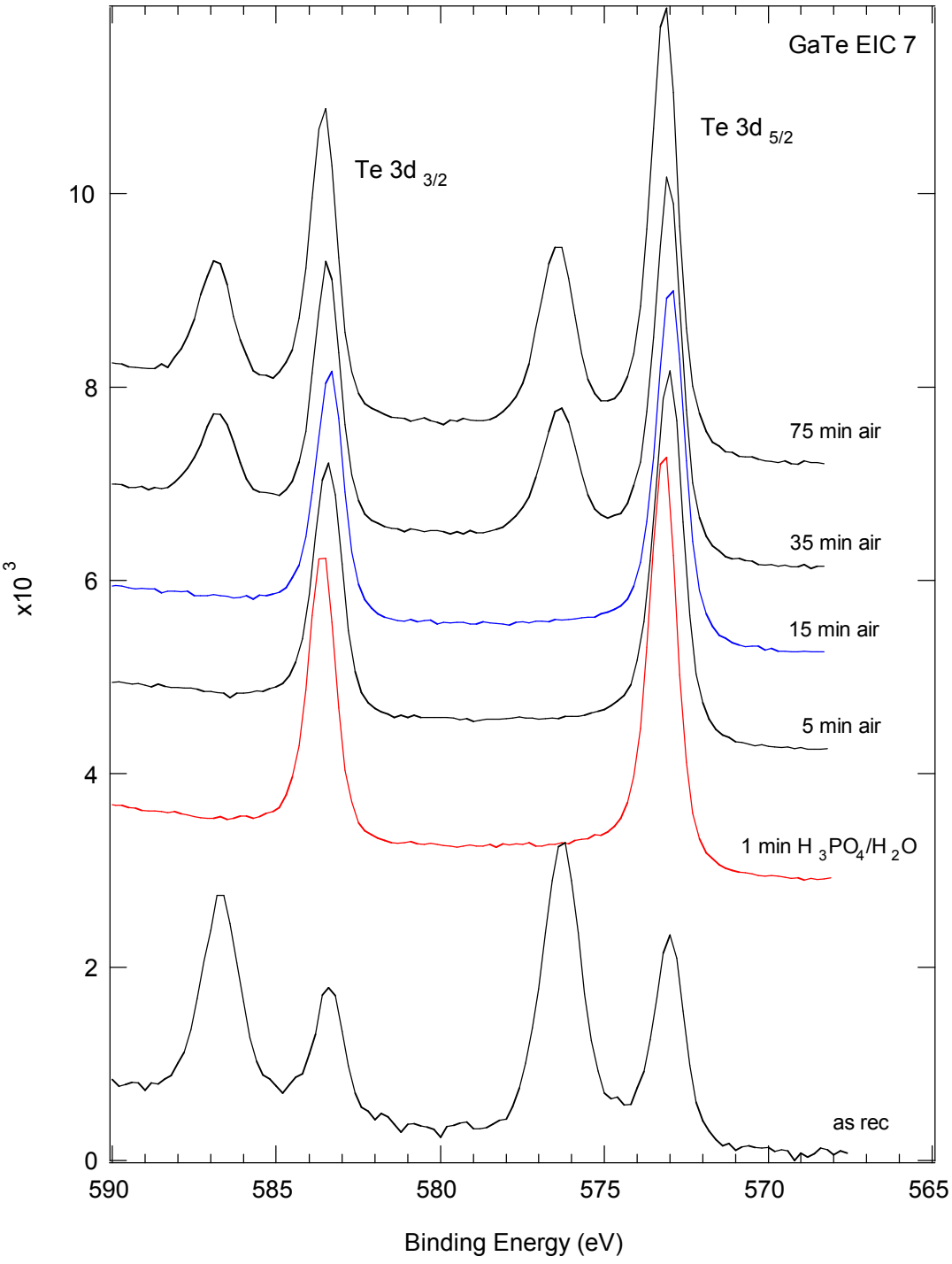
GaTe EIC 7
Te 3d 5/2
Te 3d 3/2
75 min air
35 min air
15 min air
5 min air
1 min H 3PO4/H 2O
as rec
x10 3
0
2
4
6
8
10
590
585
580
575
570
565
Binding Energy (eV)

Figure 4

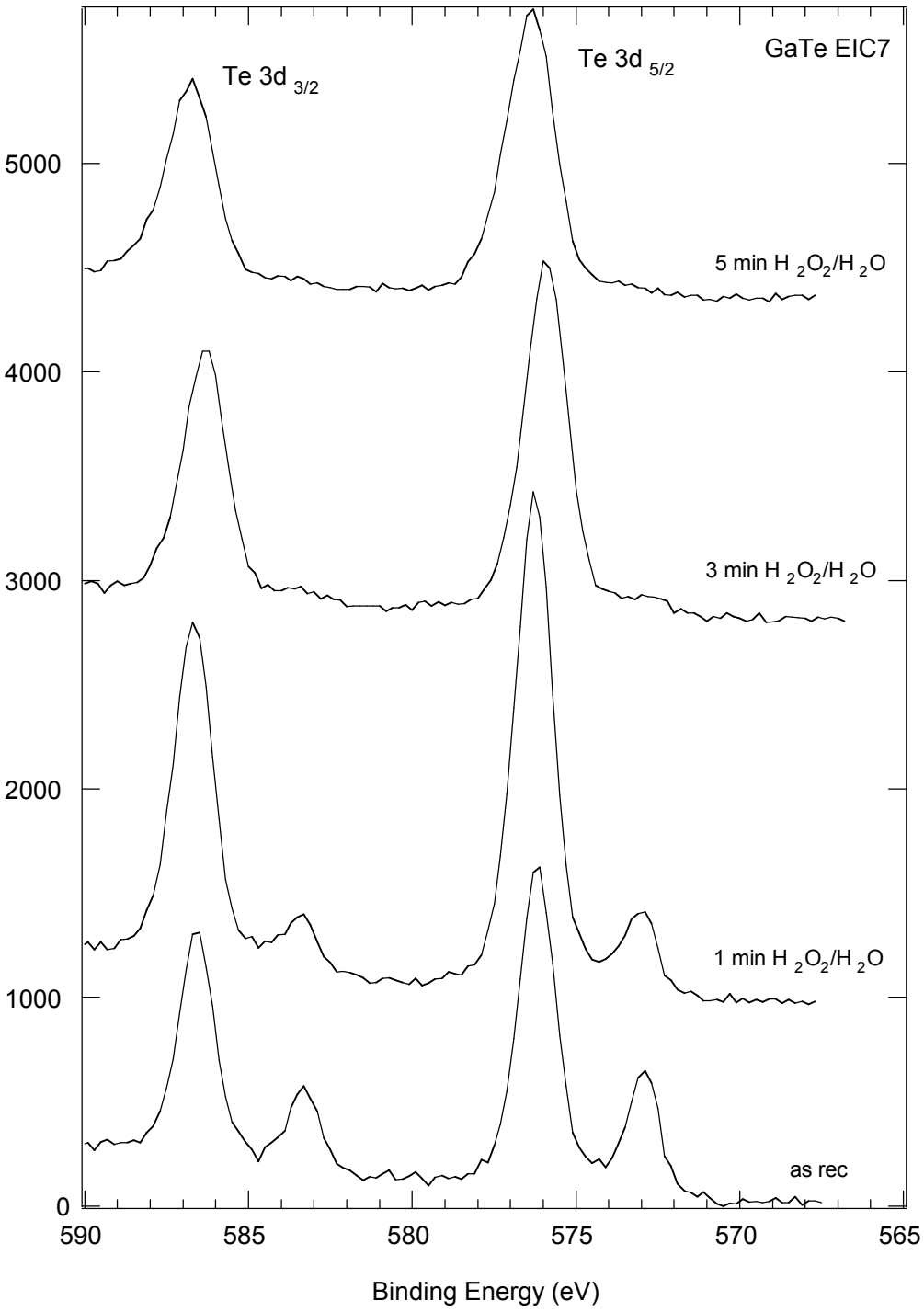
Te 3d 3/2
Te 3d 5/2
GaTe EIC7
5000
4000
3000
2000
1000
0
5 min H 2O2/H 2O
3 min H 2O2/H 2O
1 min H 2O2/H 2O
as rec
590
585
580
575
570
565
Binding Energy (eV)

Figure 5.

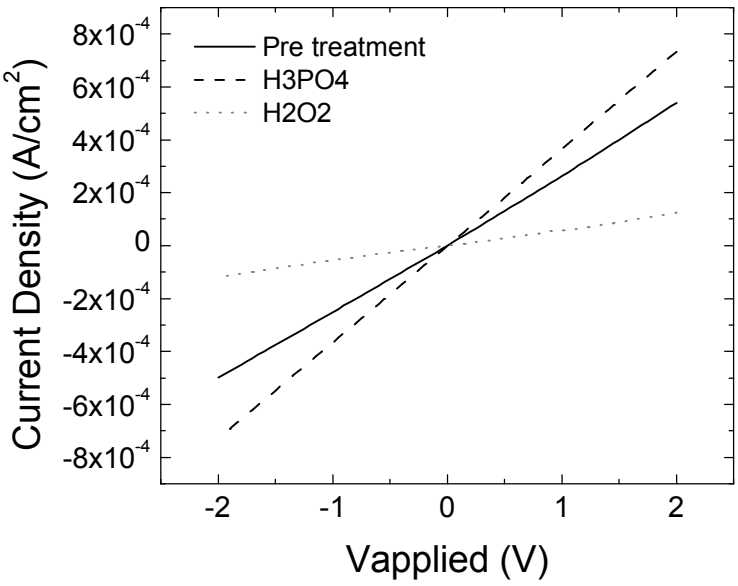
Pre treatment
H3PO4
H2O2
Current Density (A/cm^2)
8x10^{-4}
6x10^{-4}
4x10^{-4}
2x10^{-4}
0
-2x10^{-4}
-4x10^{-4}
-6x10^{-4}
-8x10^{-4}
-2
-1
0
1
2
Vapplied (V)

Figure 6.

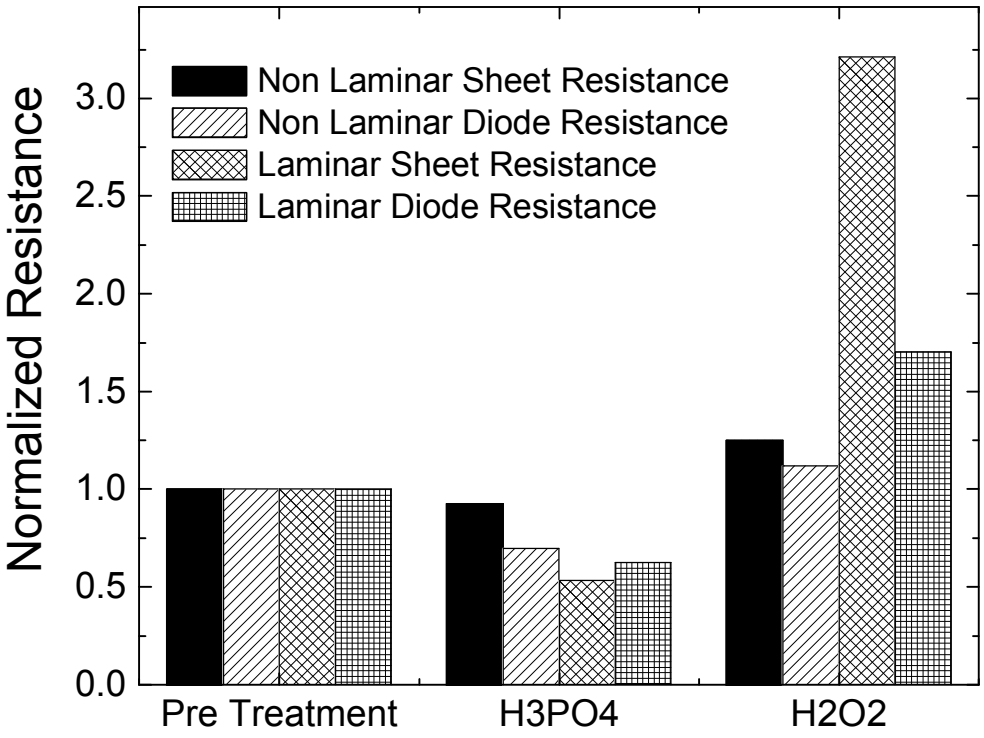
Normalized Resistance
0.0
0.5
1.0
1.5
2.0
2.5
3.0
Non Laminar Sheet Resistance
Non Laminar Diode Resistance
Laminar Sheet Resistance
Laminar Diode Resistance
Pre Treatment
H3PO4
H2O2

Figure 7. P/A ratio

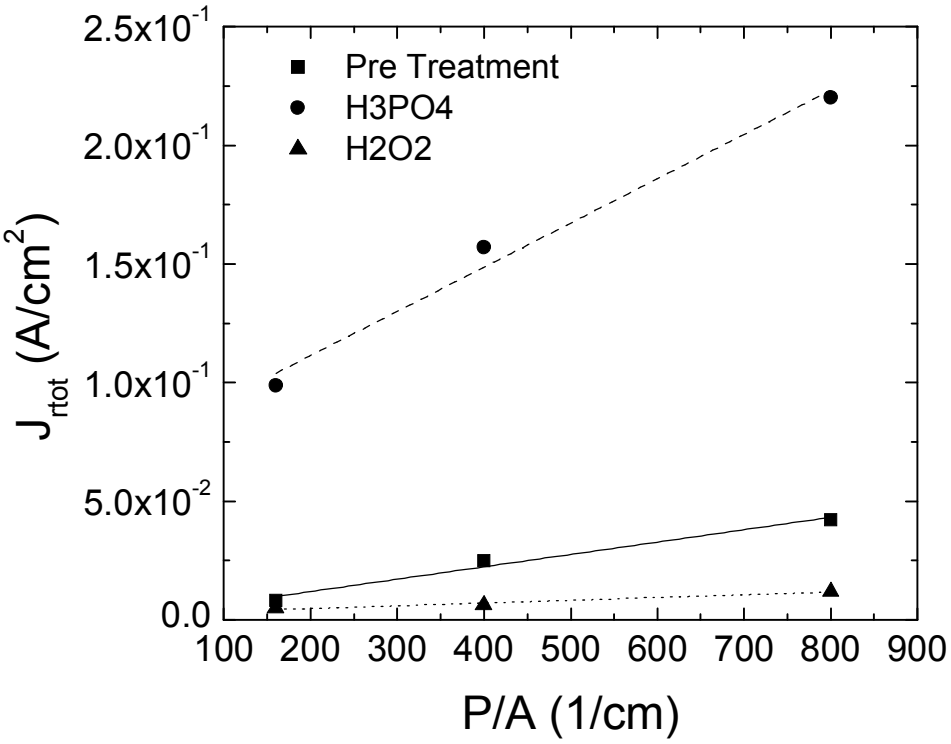

Figure 8.

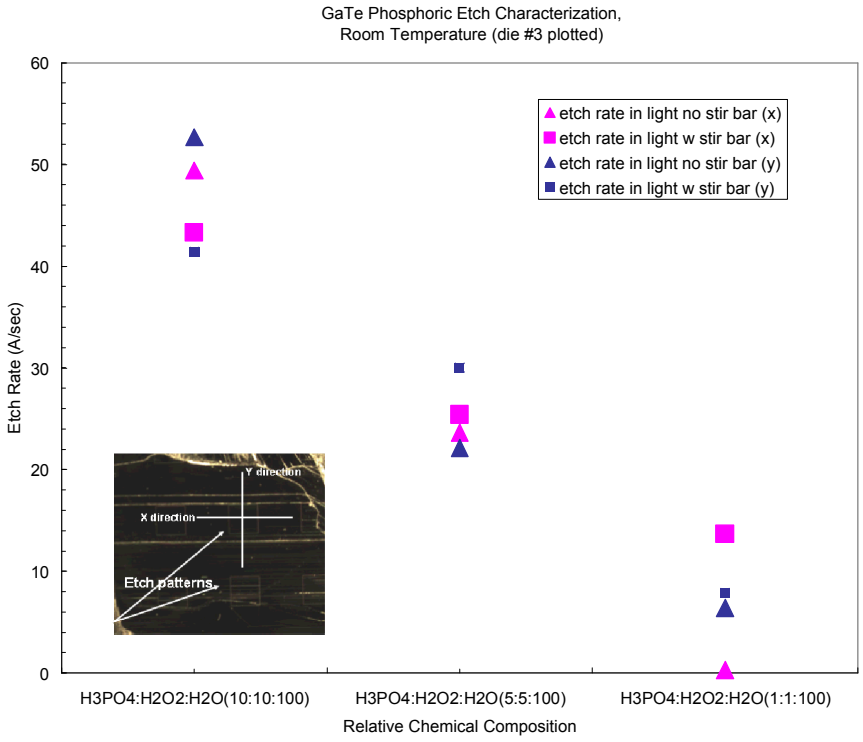

Figure 9.